Bioactive Materials 5 (2020) 694–708

Contents lists available at ScienceDirect

Bioactive Materials

journal homepage: http://www.keaipublishing.com/biomat

Targeted delivery of chlorogenic acid by mannosylated liposomes to effectively promote the polarization of TAMs for the treatment of glioblastoma

Jun Ye[a,b,1], Yanfang Yang[a,b,1], Jing Jin[a], Ming Ji[a], Yue Gao[a,b], Yu Feng[a,b], Hongliang Wang[a,b], Xiaoguang Chen[a,*], Yuling Liu[a,b,**]

[a] State Key Laboratory of Bioactive Substance and Function of Natural Medicines, Institute of Materia Medica, Chinese Academy of Medical Sciences & Peking Union Medical College, Beijing, 100050, PR China

[b] Beijing Key Laboratory of Drug Delivery Technology and Novel Formulation, Institute of Materia Medica, Chinese Academy of Medical Sciences & Peking Union Medical College, Beijing, 100050, PR China

ARTICLE INFO

Keywords:
Chlorogenic acid
Mannosylated liposome
Tumor-associated macrophage
Cancer immunotherapy
Drug delivery

ABSTRACT

Tumor-associated macrophages (TAMs) generally display an immunosuppressive M2 phenotype and promote tumor progression and metastasis, suggesting their potential value as a target in cancer immunotherapy. Chlorogenic acid (CHA) has been identified as a potent immunomodulator that promotes the polarization of TAMs from an M2 to an M1 phenotype. However, rapid clearance in vivo and low tumor accumulation have compromised the immunotherapeutic efficacy of CHA in clinical trials. In this study, mannosylated liposomes are developed for targeted delivery of CHA to TAMs. The immunoregulatory effects of CHA, along with the overall antitumor efficacy of CHA-encapsulated mannosylated liposomes, are investigated through in vitro and in vivo experiments. The prepared CHA-encapsulated mannosylated liposomes exhibit an ideal particle size, favorable stability, and preferential accumulation in tumors via the mannose receptor-mediated TAMs-targeting effects. Further, CHA-encapsulated mannosylated liposomes inhibit G422 glioma tumor growth by efficiently promoting the polarization of the pro-tumorigenic M2 phenotype to the anti-tumorigenic M1 phenotype. Overall, these findings indicate that CHA-encapsulated mannosylated liposomes have great potential to enhance the immunotherapeutic efficacy of CHA by inducing a shift from the M2 to the M1 phenotype.

1. Introduction

Glioblastoma (GBM), the most aggressive and common malignant primary brain tumor, carries a bleak prognosis despite aggressive treatment [1]. There is evidence that the tumor microenvironment plays a key role in promoting the tumor growth and progression of GBM [2]. As a dominant population of infiltrating immune cells in tumor microenvironments, tumor-associated macrophages (TAMs) have been confirmed to promote tumor growth, angiogenesis, progression, metastasis, and immune suppression [3,4]. The critical role of TAMs in promoting GBM growth is highlighted by the largest proportion of tumor-infiltrating cells within GBM, comprising up to 50% of all cells of the tumor mass [5]. Given the importance of TAMs in regulating tumor progression, there has been considerable interest in TAMs-centred cancer immunotherapy strategies for the treatment of GBM [4,6–8].

With advances in nanomedicine, the design of TAMs-targeted nanocarriers opens doors for targeted delivery of immunomodulators to selectively eliminate or promote polarization of TAMs infiltrating tumor environment [4,7]. A distinguishing feature of TAMs during M2 polarization is their enhanced expression of mannose receptors, a C-type lectin [9]. The mannose receptors involve eight extracellular carbohydrate-recognition domains, which can recognize repeated mannose residues [10]. The substantial expression of mannose receptors on TAMs was extensively explored for the design of TAMs-targeting

Peer review under responsibility of KeAi Communications Co., Ltd.

* Corresponding author. State Key Laboratory of Bioactive Substance and Function of Natural Medicines, Institute of Materia Medica, Chinese Academy of Medical Sciences & Peking Union Medical College, 1 Xiannongtan Street, Beijing, 100050, PR China.

** Corresponding author: State Key Laboratory of Bioactive Substance and Function of Natural Medicines, Institute of Materia Medica, Chinese Academy of Medical Sciences & Peking Union Medical College, 1 Xiannongtan Street, Beijing, 100050, PR China.

E-mail addresses: chxg@imm.ac.cn (X. Chen), ylliu@imm.ac.cn (Y. Liu).

[1] Jun Ye and Yanfang Yang contributed equally to this work.

https://doi.org/10.1016/j.bioactmat.2020.05.001
Received 15 March 2020; Received in revised form 6 May 2020; Accepted 7 May 2020
2452-199X/ © 2020 Production and hosting by Elsevier B.V. on behalf of KeAi Communications Co., Ltd. This is an open access article under the CC BY-NC-ND license (http://creativecommons.org/licenses/BY-NC-ND/4.0/).

nanocarriers [7,11,12]. In our previous study, liposomes modified with mannose exhibited superior in vitro cellular internalization, tumor spheroid penetration, and in vivo tumor accumulation with the aid of mannose receptor-mediated TAMs-targeting effects [13]. In particular, drug-free mannosylated liposomes inhibited GBM tumor growth by promoting the polarization of TAMs toward the anti-tumorigenic M1 phenotype in vivo [13]. The polarization of TAMs induced by drug-free nanocarriers may be associated with suppressing STAT6 and activating NF-κB phosphorylation [10,13]. However, this interesting result is inconsistent with that reported in the literature: drug-free PEGylated liposomes could induce polarization of TAMs toward the pro-tumorigenic M2-phenotype and then lead to tumor progress and immunosuppression in TC-1 cervical cancer models [14,15]. Although differences in physicochemical properties of liposomes may contribute to the aforementioned contradictory results, the substantial heterogeneity in tumor microenvironment among different types of tumors may be the culprit [15,16]. Due to a considerable amount of TAMs infiltrating within GBM, mannosylated liposomes may deeply interrupt the biological interactions between TAMs, tumor cells, and other cells with the aid of mannose receptor-mediated TAMs-targeting effects, consequently modulate the polarization of TAMs. Based on the above findings and the substantial expression of mannose receptors on TAMs [7,17–20], mannosylated liposome is an attractive choice for targeted delivery of immunomodulators to TAMs for the treatment of GBM.

Chlorogenic acid (CHA) has been reported to possess multiple beneficial pharmacological activities [21,22]. Our previous study found that CHA functions as an antitumor immunomodulator that promotes the polarization of TAMs from the M2 to the M1 phenotype via the promotion of STAT1 activation and the inhibition of STAT6 activation, thereby modulating the tumor microenvironment and inhibiting the growth of GBM[6]. Recently, CHA has completed a phase I clinical trial and is now entering a phase II clinical trial in glioma patients. The phase I clinical trial report demonstrated that CHA injections in patients with recurrent high-grade GBM were safe, well-tolerated, and conferred potential antitumor effects [23]. Overall, these pre-clinical and clinical results make CHA an attractive candidate for cancer immunotherapy. However, as a small-molecule compound, CHA is rapidly cleared in vivo following injection, thereby resulting in a short circulation time and low tumor accumulation [24,25]. Although the antitumor efficacy was satisfactory in the clinical trial after intramuscular injection daily for months, poor patient compliance makes the treatment difficult to administer.

To overcome the limitations mentioned above, targeted delivery of CHA via mannosylated liposomes holds great promise. Herein, we developed mannosylated liposomes to encapsulate CHA for targeted delivery of CHA to TAMs for cancer immunotherapy (Scheme 1). To improve the lipophilicity of CHA and facilitate its association with liposomes, a CHA-phospholipid complex was developed as an intermediate [26]. The physicochemical properties, targeted delivery capability, M2 phenotype TAMs repolarization ability, tissue distribution, and antitumor efficacy of CHA-encapsulated mannosylated liposomes were systematically evaluated on macrophages in vitro and against a G422 glioma tumor model in vivo. These results present a potential new approach for TAMs-centred cancer immunotherapy that efficiently delivers CHA to TAMs and enhances the antitumor immune efficacy of CHA based on a shift from the M2 to the M1 phenotype with negligible systemic toxicity.

2. Material and methods

2.1. Materials

Soybean phosphatidylcholine S100 was purchased from Shanghai Tywei Pharmaceutical Co., Ltd. (Shanghai, China). Cholesterol, DSPE-PEG_{2000}, and DSPE-PEG_{2000}-NHS were purchased from A.V.T. Pharmaceutical Co., Ltd. (Shanghai, China). Chlorogenic acid was provided by Sichuan Jiuzhang Biotech Co., Ltd. (Chengdu, Sichuan, China). Mannose, temozolomide, and 4-aminophenyl α-D-mannopyranoside were obtained from J&K Scientific Ltd. (Beijing, China). Coumarin-6 was purchased from Sigma-Aldrich (Saint Louis, MO, USA). DiR was purchased from AAT Bioquest, Inc. (Sunnyvale, CA, USA). The iNOS primer was obtained from Sino Biological Inc. (Beijing, China). Recombinant murine macrophage colony stimulating factor (M-CSF) and recombinant murine interleukin-4 (IL-4) were supplied by PeproTech (Rocky Hill, NJ, USA). Dulbecco's Modified Eagle's Medium (DMEM) and fetal bovine serum (FBS) were purchased from Thermo Fisher Scientific Inc. (Waltham, MA, USA). All other organic reagents were of analytical grade and were purchased from Sinopharm Chemical Reagent Co., Ltd. (Shanghai, China).

2.2. Cell culture

The RAW264.7 murine macrophage cell line was obtained from the Cell Resource Center, Peking Union Medical College (Beijing, China). The G422 murine glioma cell line was provided by Beijing Neurosurgical Institute (Beijing, China). RAW264.7 and G422 cells were cultured in DMEM supplemented with 10% FBS, 100 U/mL penicillin, and 100 μg/mL streptomycin in a humidified atmosphere of 5% CO_2 at 37 °C.

2.3. Isolation and polarization of BMDMs

Bone marrow derived macrophages (BMDMs) were generated from bone marrow progenitors isolated from both femurs and tibias of C57BL/6 mice, as previously described [27]. The harvested bone marrow cells were grown in DMEM culture medium supplemented with 20 ng/mL recombinant M-CSF for 7 days to facilitate differentiation into naïve macrophages (BMDMs). After differentiation, BMDMs were collected, and macrophage marker expressions (F4/80) were determined using flow cytometry. BMDMs were polarized into M2 subtypes through stimulation with 20 ng/mL IL-4 for 24 h (Fig. 3A).

2.4. Preparation and characterization of liposomes

DSPE-PEG_{2000}-Mannose (DSPE-PEG_{2000}-Man) was synthesized using DSPE-PEG_{2000}-NHS and 4-aminophenyl α-D-mannopyranoside, according to the methodology previously described [13], and the chemical structure was characterized using ^{1}H nuclear magnetic resonance (NMR).

The CHA-phospholipid complex was prepared using a solvent evaporation method. CHA and phospholipids (1:2.2, w/w) were dissolved in absolute ethanol and magnetically stirred for 15 min at room temperature. A solid was obtained after the organic solvent was removed under agitation and vacuum. The resulting CHA-phospholipid complex was weighed (XS105DU; Mettler-Toledo GmbH, Zurich, Switzerland) and stored at −20 °C until further use. Liposomes were prepared by the thin-film hydration method, as described in our previous study [13]. In brief, lipids, including S100, cholesterol, and DSPE-PEG_{2000}-Man, were dissolved in chloroform, and the pre-weighed CHA-phospholipid complex was added. The organic solvent was removed by rotary evaporation under vacuum to form a thin film layer. The lipid film was hydrated in phosphate buffered saline (PBS; pH 5.5) and was intermittently sonicated to obtain mannosylated liposomes (Man-PEG-Lipo). Conventional bare liposomes (Lipo) and PEGylated liposomes (PEG-Lipo) were prepared as described above, except that the molar ratio of lipids varied accordingly. Liposomes loaded with DiR or coumarin-6 were prepared using a similar procedure, except that DiR or coumarin-6 was dissolved in chloroform along with the lipids. The entrapment efficiency of CHA in the liposomes was determined by the centrifugation ultrafiltration method. The mean particle size and size distribution of liposomes were measured by the dynamic light scattering (DLS) method. The morphology of liposomes was observed by

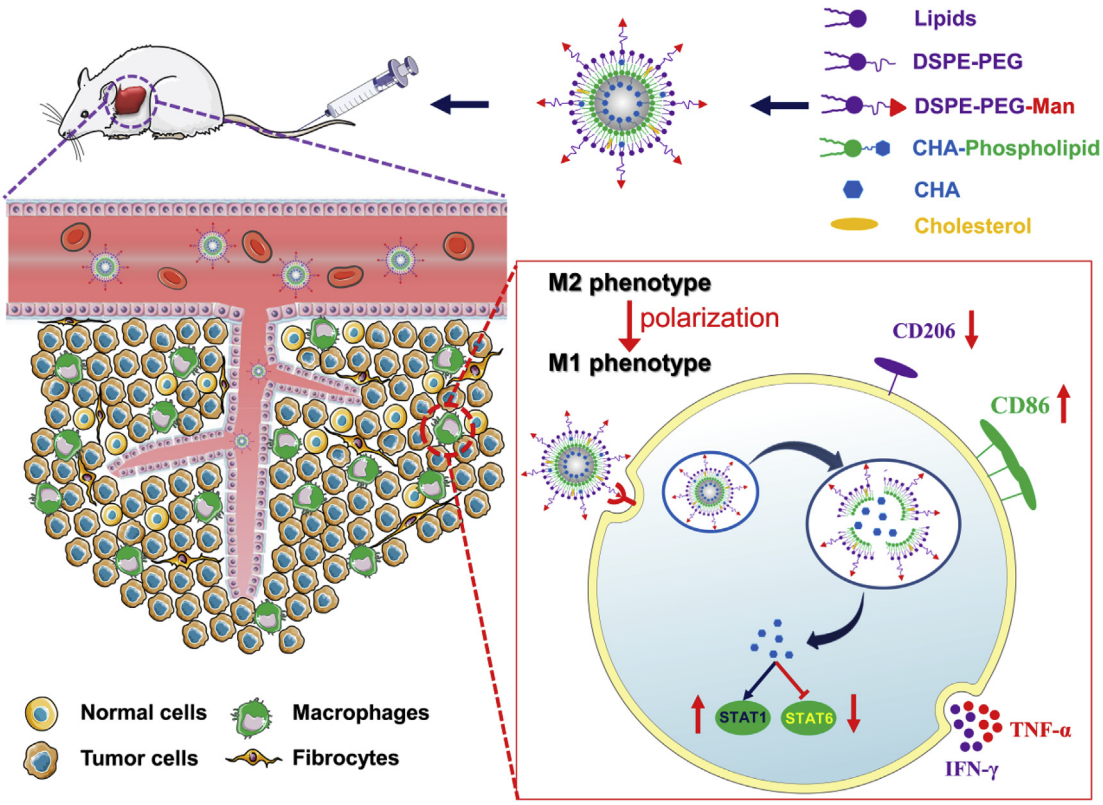

Scheme 1. Schematic overview of CHA-encapsulated Man-PEG-Lipo that enhances tumor accumulation via active targeting to mannose receptor-expressing TAMs and promotes the polarization of TAMs for cancer immunotherapy.

transmission electron microscopy (TEM) (H-7650; Hitachi, Tokyo, Japan). Samples were prepared by adding one drop of liposome suspension to a copper grid followed by staining with 2% (w/w) phosphotungstic acid. The samples were then dried and examined.

2.5. Turbiscan stability index

The in vitro physical stability of liposomes in PBS at 4 ˚C or in culture medium with 10% FBS at 37 ˚C was qualitatively determined by Turbiscan Tower® (Formulaction, L'Union, France) using multiple light scattering. The liposomes were appropriately diluted in the medium, placed into a cylindrical glass cell, and scanned by the light source from bottom to top. The transmission intensity profiles as a function of position were acquired over a scan. The variation of average transmitted intensity (ΔT) and turbiscan stability index (TSI) calculated from the signal value of transmission light were used as important parameters to judge the stability of the liposomes in medium [28].

2.6. In vitro cytotoxicity

The in vitro cytotoxicity of Lipo, PEG-Lipo, and Man-PEG-Lipo was evaluated in RAW264.7 macrophages using CCK-8 kits (Dojindo Laboratories, Tokyo, Japan). RAW264.7 cells or M2-type BMDMs were plated at a density of 1×10^4 cells per well in a 96-well plate. After 24 h, the cells were treated with different liposome samples containing various concentrations of CHA (0, 0.01, 0.1, 1, and 10 μM). After incubation for 24 h, the number of viable cells was determined using CCK-8 kits, according to the manufacturer's protocol. Untreated cells were used as the control and were considered to be 100% viable.

2.7. In vitro cellular uptake

The cellular uptake profiles of the different liposomes loaded with coumarin-6 were evaluated by flow cytometry. Briefly, BMDMs were seeded into 6-well plates at a density of 5×10^5 cells per well and incubated for 24 h. Then, the cells were pretreated with IL-4 (20 ng/mL) for 24 h, followed by incubation with coumarin-6-encapsulated liposome at 37 ˚C. After incubation for 1 h, the cells were harvested, washed three times with cold PBS, and then analyzed using a flow cytometer (Accuri C6; BD Biosciences, San Jose, CA, USA). To further confirm the potential of mannose receptors to mediate the uptake of Man-PEG-Lipo, M2-type BMDMs were treated with Man-PEG-Lipo and excess mannose (100 mM) [][56], individually or in combination, followed by flow cytometer analysis.

2.8. Polarization of M2 macrophages in vitro

BMDMs were seeded in 6-well plates at a density of 5×10^5 cells per well and were stimulated with IL-4 for 24 h in order for them to differentiate into M2 macrophages. M2-type BMDMs were then treated with Man-PEG-Lipo at a concentration of 1 μM CHA for 24 h, followed by incubation with antibodies of M2-type BMDMs surface markers (CD206 for M2-type; BioLegend; San Diego, CA, USA). After incubation and rinsing, the samples were analyzed using flow cytometry.

2.9. Pharmacokinetic study and tissue biodistribution in vivo

Female ICR mice weighing 18–20 g were supplied by SPF (Beijing) Biotechnology Co., Ltd. (Beijing, China). All animal experiments were approved by the Institutional Animal Care and Use Committee of Peking Union Medical College. For plasma pharmacokinetic study, female ICR mice were randomly divided into two groups (free CHA and Man-PEG-Lipo, n = 3 per group) to receive free CHA solution or Man-PEG-Lipo with equivalent CHA doses of 40 mg/kg via single intravenous injection. Blood samples were collected and analyzed for CHA content using HPLC–MS/MS (6480B; Agilent Technologies). For

tissue biodistribution study, the glioma tumor model was established through the subcutaneous injection of 2×10^6 G422 cells to the right flank of each ICR mouse. When the tumors grew to a median size of 500 mm^3, DiR-encapsulated liposomes were injected into the tail vein of each mouse (0.1 mg/kg body weight). During the experiment, whole-body fluorescence images were taken at predetermined times post-injection (2, 4, 6, 8, 12, and 24 h) using the In Vivo IVIS spectrum-imaging system (PerkinElmer, Waltham, MA, USA). At the end of the experiment, the mice were euthanized, and the tumors and other major organs were surgically collected. These were then examined using ex vivo imaging.

2.10. In vivo antitumor efficacy and safety evaluation

The glioma tumor model was established in female ICR mice, as mentioned above. The tumor-bearing mice were randomly divided into six groups (control, TMZ, CHA, Lipo, PEG-Lipo, and Man-PEG-Lipo, n = 6–7 per group) the day after tumor implantation. The TMZ group (positive control group) was orally treated with temozolomide (TMZ) (50 mg/kg) for 5 days. The other groups were intravenously injected with free CHA solution (CHA group) or different liposomes (Lipo, PEG-Lipo, and Man-PEG-Lipo groups) with equivalent CHA doses of 20 mg/kg, daily or once every other day for about two weeks. The schedule of administration is illustrated in Figs. 6A and 7A. Bodyweight and tumor volume were measured for each mouse to evaluate in vivo safety and antitumor efficacy, respectively. The tumor volume was calculated according to the following formula: tumor volume = length × $(width)^2$/2. At the end of the experiments, all mice were euthanized, and the tumors were collected, weighed, and photographed. The tumor growth inhibition ratio (TGI%) was calculated by the following formula: TGI% = $(1\text{-}W_{test}/W_{vehicle}) \times 100$, where W_{test} and $W_{vehicle}$ represent the tumor weight of treatment group and vehicle group, respectively. At the end of the in vivo antitumor experiment with interval administration, the fresh tumor, spleen, and peripheral blood were collected and further analyzed to evaluate the in vivo polarization ability of CHA-encapsulated liposomes. Hematological examination was performed with an automatic hematology analyzer (MEK-7222 K; Nihon Kohden, Tokyo, Japan).

2.11. Polarization ability of liposomes in vivo

The in vivo polarization ability of CHA-encapsulated liposomes was evaluated by analyzing the ratio of M1/M2 subtype macrophages, cytokine production, and the expression profiles of surface proteins and gene markers. The ratio of M1/M2 subtype macrophages infiltrated into tumors and spleens was quantitatively analyzed using flow cytometry. The fresh tumors and spleens were cut into small pieces and then digested for 40 min at 37 °C to obtain cell suspensions. The red blood cells were removed using a red blood cell lysis buffer. The cells were collected, washed, and were incubated with APC antimouse CD45, FITC antimouse CD11b, Brilliant Violet 605™ antimouse F4/80, Brilliant Violet 421™ antimouse CD206 (M2-type), and PE antimouse CD11c (M1-type) (BioLegend; San Diego, CA, USA). The cell suspensions were filtered through 400 mesh sieves after being washed twice and were then analyzed using flow cytometry (NovoCyte D3010; AECA Biosciences, San Diego, CA, USA). The $CD45^+CD11b^+F4/80^+CD206^+$ cells and $CD45^+CD11b^+F4/80^+CD11c^+$ cells were considered to be M2-type and M1-type TAMs, respectively [29,30]. The different cytokines (IFN-γ, TNF-α, and IL-10) in tumors, spleens, and blood were quantitatively determined by bead-based LEGENDplex™ assays (BioLegend; San Diego, CA, USA) according to the manufacturer's protocol. For immunofluorescence assays, the tumors were fixed with 4% paraformaldehyde, embedded with paraffin, and dissected. After that, the DAPI, F4/80, CD86, and CD206 were stained. Images were obtained by confocal laser scanning microscopy. Besides, the expression profile of a gene marker (iNOS mRNA) was analyzed by quantitative real-time PCR.

2.12. Statistical analyses

All data subjected to statistical analyses were obtained from at least three parallel experiments, and the results are expressed as mean ± standard error of mean (SEM). The statistical analysis was performed by Student's t-tests for two groups, and one way ANOVA for multiple groups using GraphPad Prism version 7.00 for Windows (GraphPad Software, La Jolla, CA, USA). A p-value ≤ 0.05 was considered to be statistically significant.

3. Results and discussion

3.1. Properties and characteristics of liposomes

The mannose receptor, also known as CD206, is one of the most commonly used TAMs-targeted receptors due to its high expression level on the surface of M2-type TAMs [31]. In the present study, the conjugation of mannose to $DSPE\text{-}PEG_{2000}$ was used as an M2-type TAMs-targeted ligand, based on the specific recognition between mannose and the mannose receptors of M2-type TAMs. $DSPE\text{-}PEG_{2000}$-Man was synthesized via NHS covalent coupling with the amino group (Fig. S1A), and the chemical structure of the obtained product was confirmed using ^1H NMR (Fig. S1B). Mannose moiety in $DSPE\text{-}PEG_{2000}$-Man was verified by the proton signals of the phenyl group at 6.9–7.5 ppm.

The overexpression profile of the mannose receptors on TAMs prompted extensive utilization of mannose ligands for decoration of nanocarriers to target TAMs via specific recognition and internalization [4]. In the present study, liposomes functionalized with $DSPE\text{-}PEG_{2000}$-Man (Man-PEG-Lipo) were developed to be potential drug carriers to target M2-like TAMs. As shown in Fig. 1, the mean particle sizes and zeta potentials of Lipo, PEG-Lipo, and Man-PEG-Lipo were 175.9 ± 1.7 nm, 139.4 ± 0.4 nm, 139.0 ± 0.5 nm, and −5.0 ± 0.5 mV, −10.2 ± 0.1 mV, −25.3 ± 0.8 mV, respectively. All liposomes exhibited low polydispersity index (PDI) values (< 0.3), indicating that the size distributions of all liposomes were narrow. TEM images of the liposomes revealed that the three kinds of liposomes were approximately spherical nanosized particles with a core-shell structure. The entrapment efficiency (EE) of CHA in Lipo, PEG-Lipo, and Man-PEG-Lipo were 71.9%, 72.7%, and 71.5%, respectively. CHA is a highly water-soluble compound that cannot be loaded effectively into liposomes with a relatively low EE of about 20%. Thus, the increased entrapment efficiency may be attributed to the enhanced lipophilicity of CHA-phospholipid complex [26].

3.2. In vitro physical stability of liposomes

The storage stability against dispersion media and the colloidal stability against physiological conditions were important aspects to be taken into account in order to effectively propose liposomes as possible carriers for the targeted delivery of therapeutics [32,33]. The in vitro storage and colloidal stabilities of the three kinds of liposomes were evaluated using the Turbiscan Lab® Expert, an advanced analyzer that can detect early imperceptible changes in transmission or backscattering profiles before the appearance of macroscopic physical modifications to nanosized colloidal suspensions [34].

The variation of the droplet volume fraction (migration) or size (coalescence) was observed as a variation of light transmission (ΔT) profiles. It can be assumed that variations greater than 10% are representative of an unstable formulation [35]. As shown in Fig. 2A and C, the variations of transmission profiles (ΔT) of both PEG-Lipo and Man-PEG-Lipo were less than 10%, indicating that there was no apparent aggregation or sedimentation when the liposomes were dispersed in PBS (4 °C) for 7 days or in culture medium (37 °C) for 24 h. On the contrary, flocculation and sedimentation occurred when Lipo was incubated in PBS or culture medium, as evidenced by the higher ΔT

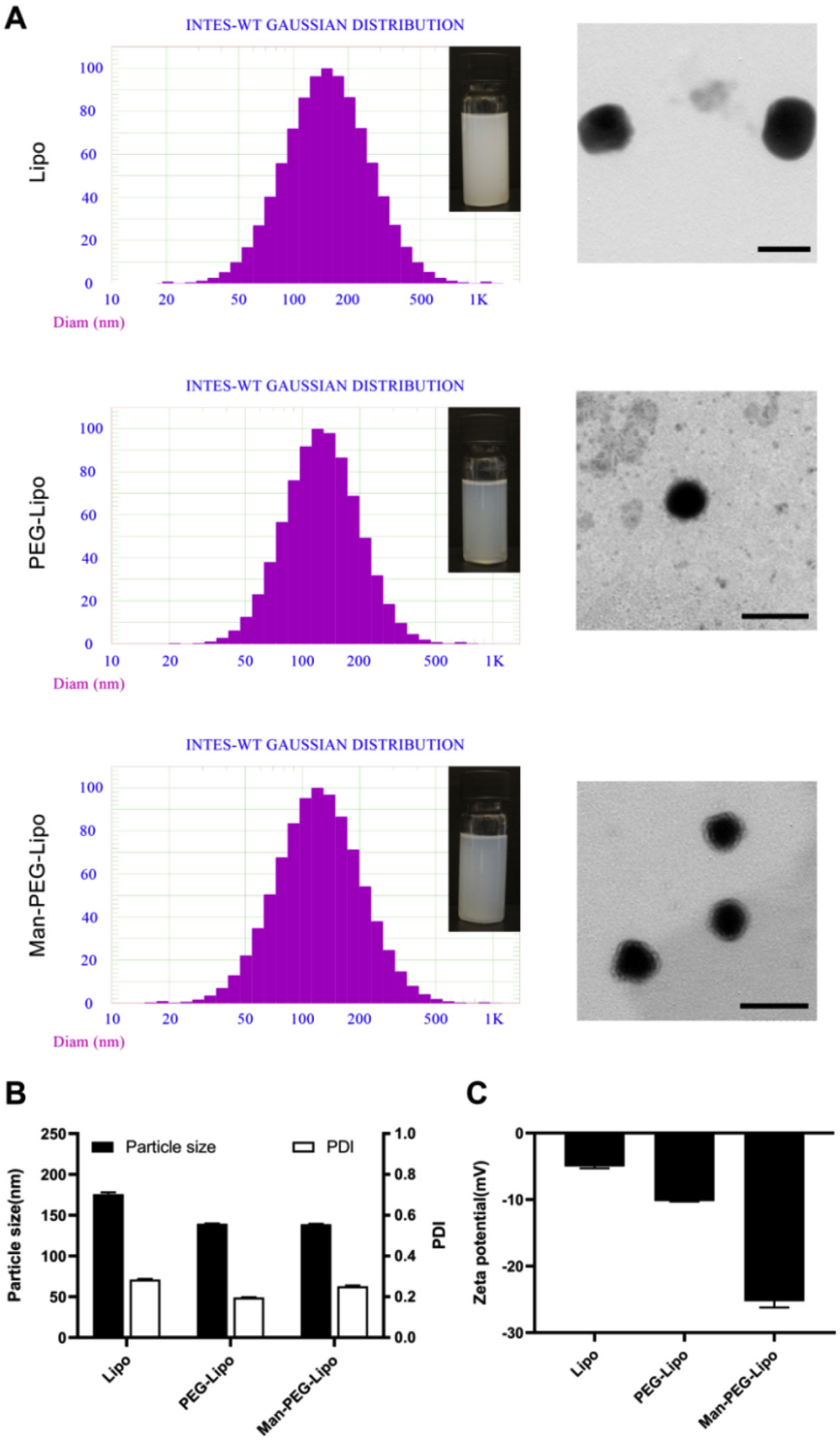

Fig. 1. In vitro characterization of liposomes. (A) Particle size distribution, appearance, and morphology of CHA-encapsulated liposomes. (B) Mean particle size and polydispersity index (PDI) of CHA-encapsulated liposomes. (C) Zeta potential of CHA-encapsulated liposomes. Each value represents the mean ± SEM (n = 3).

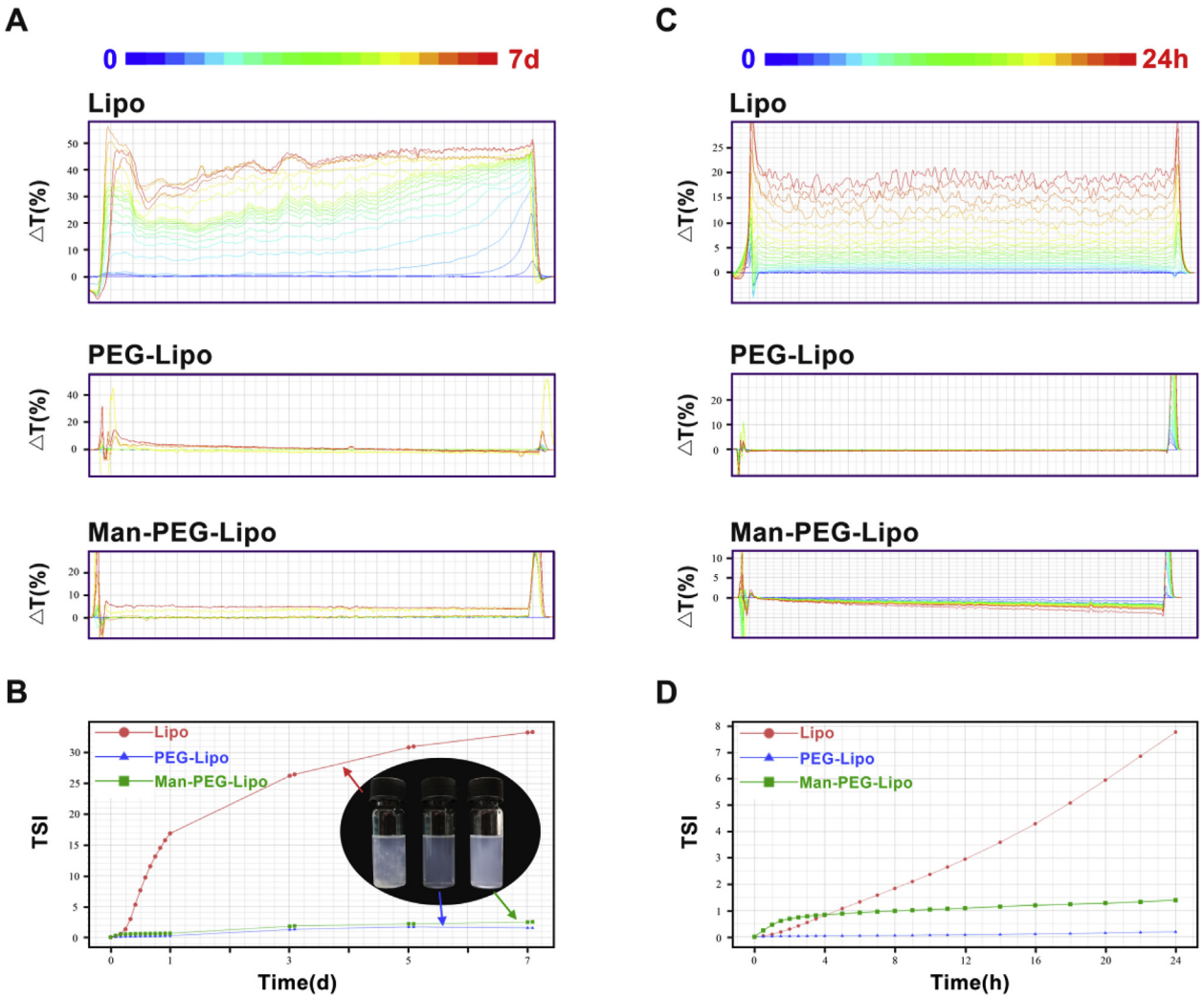

Fig. 2. In vitro physical stability of liposomes. (A) Variations of transmission profiles (ΔT) and (B) TSI of CHA-encapsulated liposomes dispersed in PBS at 4 °C for 7 days. (C) Variations of transmission profiles (ΔT) (D) TSI of CHA-encapsulated liposomes dispersed in culture medium containing 10% FBS at 37 °C for 24 h.

(above 10%) value and by their appearance. In order to compare the in vitro stabilities of liposomes more intuitively, the TSI values under different conditions were calculated from the changes in transmitted light. Larger TSI values represent less stability [36]. The TSI of Lipo increased with the extension of incubation time, while PEG-Lipo and Man-PEG-Lipo maintained relatively low TSI values (Fig. 2B and D). These results demonstrated that both PEG-Lipo and Man-PEG-Lipo possess excellent storage and colloidal stabilities, which may be attributed to the surface modification of highly hydrated groups that sterically reduce both electrostatic and hydrophobic interactions among plasma components around the PEGylated liposome surface [37]. This superior stability could prolong liposome circulation time in the blood and enhance its accumulation in tumors via enhanced permeability and retention (EPR) effects [38,39].

3.3. Cellular uptake profile of liposomes

A schematic description of the generation procedure for BMDMs is illustrated in Fig. 3A. High purity of mature BMDMs can be obtained, and the macrophages can be used for further experiments on day 7, as evidenced by the fact that 97% of cells were F4/80 positive (Fig. 3B and C). After treatment with IL-4, polarized M2-type BMDMs can be distinguished using antibodies against CD206. As shown in Fig. 3D, the expression of CD206 surface antigens on IL-4-treated BMDMs was significantly up-regulated (12.7%, about 25-fold higher) compared to the control group (0.5%), indicating the successful polarization of the BMDMs to M2-type macrophages [][56].

To investigate the mannose receptor-mediated TAMs-targeting efficiency of Man-PEG-Lipo on M2-type BMDMs, the cellular uptake profiles of coumarin-6-encapsulated liposomes were determined quantitatively by flow cytometry. As shown in Fig. 3E and G, Man-PEG-Lipo exhibited the highest mean fluorescence intensity (MFI) in M2-type BMDMs compared to PEG-Lipo and Lipo. To confirm whether this enhanced uptake by macrophages was mediated by the mannose receptors, BMDMs were firstly pretreated with IL-4 to stimulate the expression of mannose receptor (Fig. 3D) and were then incubated with excess mannose to saturate the mannose receptors. As shown in Fig. 3F and H, the cellular uptake of Man-PEG-Lipo was significantly enhanced in BMDMs pretreated with IL-4 (M2-type) compared to the control group (M0-type). Additionally, pre-incubation with excess mannose reduced the uptake of Man-PEG-Lipo in IL-4 treated BMDMs (M2-type). The uptake characteristics of Man-PEG-Lipo in BMDMs (primary macrophages) were consistent with those in RAW264.7 (macrophages cell line) [13]. These results demonstrate that mannose conjugation on the liposomes' surface effectively facilitates in vitro cellular uptake by M2-type macrophages and that the expression profiles of mannose receptors regulate the cellular uptake of Man-PEG-Lipo before and after polarization.

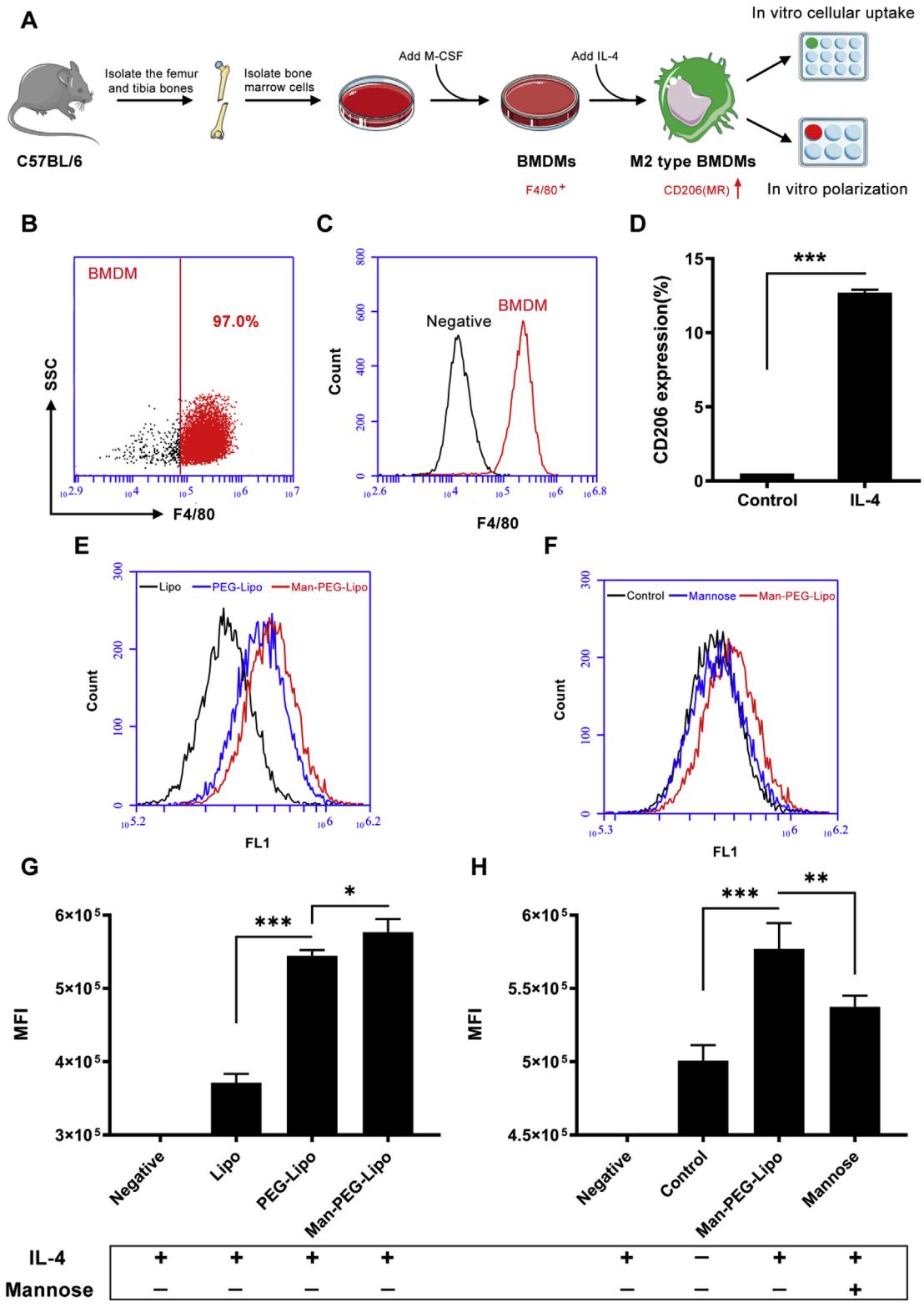

Fig. 3. In vitro cellular uptake profile of liposomes in BMDMs. (A) Scheme for the isolation, formation, and stimulation of mouse BMDMs. (B and C) Flow cytometric analysis of purity of cultured BMDMs. (D) Flow cytometric analysis of CD206 expression level of IL-4-treated BMDMs. (E and G) The cellular uptake profile of coumarin-6 labeled liposomes in M2-type BMDMs. (F and H) The cellular uptake profile of coumarin-6 labeled Man-PEG-Lipo in naïve BMDMs (Control) or M2-type BMDMs alone (Man-PEG-Lipo) or co-incubation with excess mannose (Mannose). Each value represents the mean ± SEM (n = 3). *p < 0.05, **p < 0.01, and ***p < 0.001.

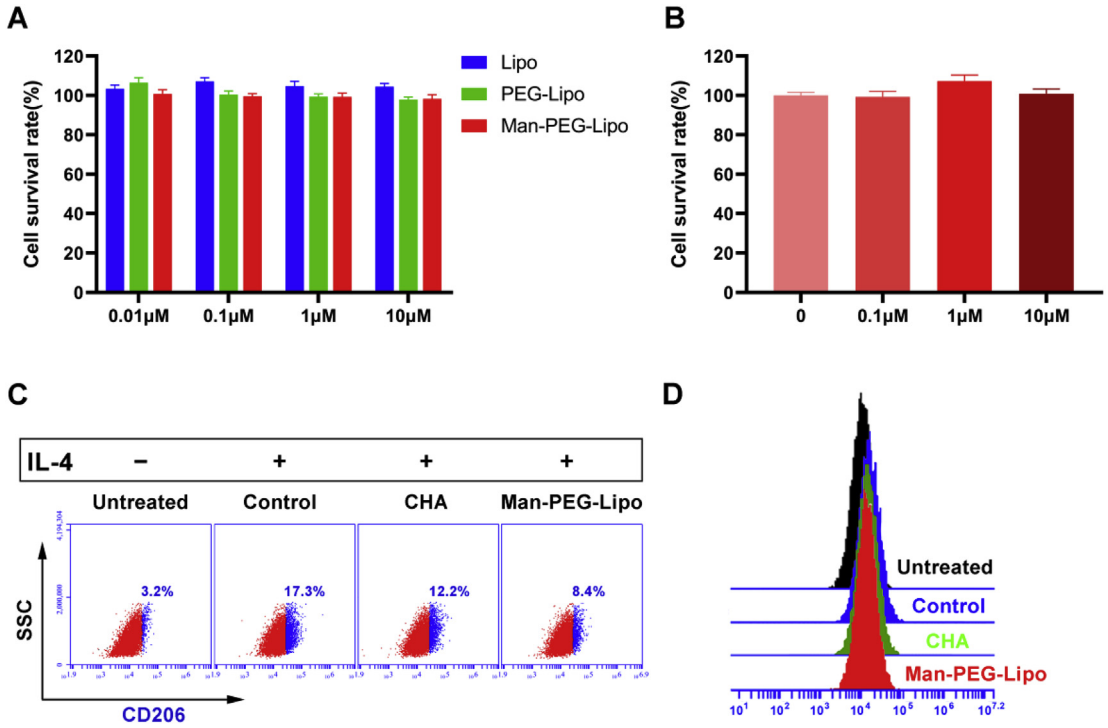

Fig. 4. Polarization of M2-type BMDMs in vitro. (A and B) In vitro cytotoxicity of liposomes in RAW264.7 and BMDMs. Each value represents the mean ± SEM (n = 3). (C and D) CD206 expression level of M2-type BMDMs after incubation with culture medium (Untreated), culture medium containing IL-4 (Control), free CHA containing IL-4 (CHA), and CHA-encapsulated Man-PEG-Lipo containing IL-4 (Man-PEG-Lipo).

3.4. In vitro cytotoxicity

As shown in Fig. 4A, the cell survival rate of all groups was near to 100% after incubation with liposomes at concentrations of CHA in the range of 0.01–10 μM for 24 h, indicating significant biocompatibility of liposomes with macrophages and there was negligible cytotoxicity to macrophages caused by CHA at a concentration of 10 μM. Similarly, CHA-encapsulated Man-PEG-Lipo at a CHA concentration lower than 10 μM produced negligible cytotoxicity to M2-type BMDMs (Fig. 4B). Our previous study found that CHA exhibited almost no direct toxicity towards either of the various human cancer cell lines at concentrations lower than 10 μM [6]. Previous studies have reported that CHA inhibits tumor growth and tumor angiogenesis in several types of malignancy by exerting its toxicity directly to tumor cells. However, the effective dose of CHA was higher than 10 μM or a maximum of 500 μM in these studies [40–43].

3.5. Polarization of M2 macrophages in vitro

In our previous study, we reported that free CHA could function as an antitumor immunomodulator that promotes the polarization of TAMs from the M2 to the M1 phenotype [6]. To further investigate the impacts of CHA-encapsulated liposomes on M2 polarization of macrophages induced by IL-4, the expression of M2 phenotype macrophage surface marker in BMDMs was determined by flow cytometry after incubation with CHA-encapsulated liposomes. Polarized macrophages are distinguished by differential receptor expression profiles: M2 phenotypic macrophages typically up-regulate the expression of CD206 [44].

As shown in Fig. 4C and D, the CD206 expression ratio significantly increased in BMDMs treated with IL-4 (Control group), indicating that IL-4 promoted the polarization of naïve macrophages to the M2 phenotype. As consistent with the results reported previously, free CHA (CHA group) was confirmed to down-regulate the CD206 expression ratio of IL-4-conditioned M2-type BMDMs in this study. In particular, CHA-encapsulated Man-PEG-Lipo (Man-PEG-Lipo group) significantly down-regulate the CD206 expression ratio of IL-4-conditioned M2-type BMDMs after incubation for 24 h. It is worth noting that Man-PEG-Lipo exhibited a trend of improved inhibition effect on the M2 polarization of macrophages induced by IL-4 compared to free CHA, which may be attributed to the dual function of active targeting and promoting polarization of mannosylated nanocarriers [13]. These results demonstrate that Man-PEG-Lipo significantly inhibits M2 polarization of macrophages and that they hold the potential to regulate the tumor microenvironment.

3.6. Tissue biodistribution in vivo

To evaluate the in vivo tumor-targeting ability of Man-PEG-Lipo, the tissue biodistribution of DiR-loaded liposomes was determined in murine G422 glioma tumor-bearing mice. As shown in Fig. 5A, the fluorescence intensity of tumor sites in DiR-Man-PEG-Lipo-treated mice was apparently higher than that in DiR-DMSO-, DiR-Lipo-, and DiR-PEG-Lipo-treated mice at all observed time points following injection with liposomes. The ex vivo fluorescent images from the excised tumors further confirmed that DiR-Man-PEG-Lipo-treated groups presented the highest fluorescence intensity as compared to the DiR-DMSO-, DiR-Lipo-, and DiR-PEG-Lipo-treated groups (Fig. 5B). Additionally, 3D reconstruction of DiR-Man-PEG-Lipo-treated mice was performed to evaluate the overall distribution of fluorescence in the tumors. As shown in Fig. 5C, the fluorescence signals were primarily distributed in the centers of the tumors. These results indicated that Man-PEG-Lipo possessed the capacity to specifically and efficiently target the tumor microenvironment and that they hold the potential to be used as an effective TAMs-targeting carrier to deliver immunomodulators to the tumor microenvironment. Since glioma-associated macrophages are the predominant inflammatory cells to infiltrate gliomas [45,46], the tumor-targeting ability of Man-PEG-Lipo may be due to their long circulation in the blood and their relatively higher uptake by TAMs with the aid of mannose receptor.

Accumulated evidence demonstrated that mannose, a glucose

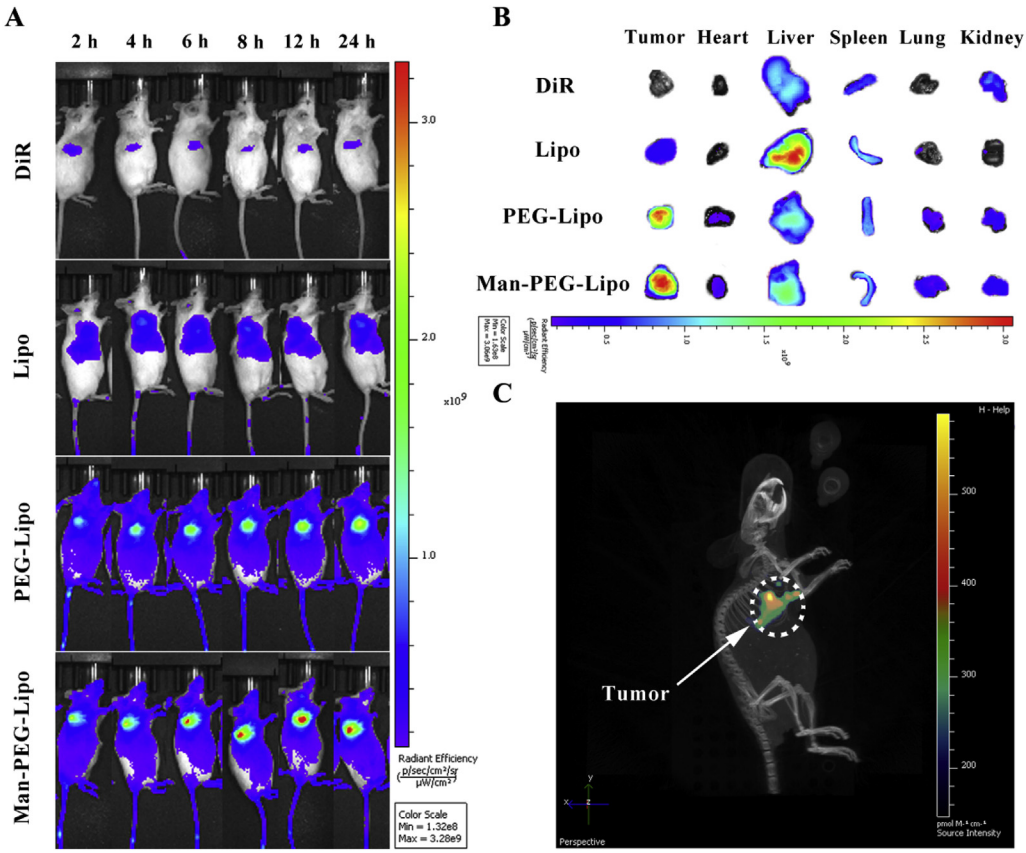

Fig. 5. In vivo biodistribution of DiR-loaded liposomes. (A) In vivo fluorescence images of ICR mice bearing G422 after tail vein injection of DiR-loaded liposomes. (B) Ex vivo fluorescence images of excised organs and tumors at 24 h post-injection of DiR-loaded liposomes. (C) 3D reconstruction of in vivo imaging of DiR-Man-PEG-Lipo-treated mice.

derivative, could traverse the blood-brain barrier through facilitative glucose transporter-mediated delivery [47–50]. Apart from the tumor sites, the brain tissue accumulation of DiR-loaded Man-PEG-Lipo was determined to evaluate the ability of Man-PEG-Lipo to cross the blood-brain barrier. As shown in Fig. S2, the fluorescence intensity of brain tissues in DiR-Man-PEG-Lipo-treated mice was greater than that in DiR-DMSO-, DiR-Lipo-, and DiR-PEG-Lipo-treated mice at all observed time points, which may be associated with the mannose mediated transport capability via the glucose transporter pathways. The in vivo ability of Man-PEG-Lipo to cross the blood-brain barrier and target the TAMs in orthotopic glioma-bearing mice will be further investigated in our future work.

3.7. In vivo antitumor efficacy of successive administration

The plasma pharmacokinetic study in ICR mice was performed to compare the pharmacokinetic characteristics of free CHA and CHA-loaded Man-PEG-Lipo. As shown in Fig. S3 and Table S1, free CHA was quickly eliminated after intravenous administration with a short half-life ($t_{1/2}$) and mean residence time (MRT) of 48.1 and 16.5 min, respectively. However, Man-PEG-Lipo exhibited altered plasma pharmacokinetics, with a longer $t_{1/2}$ and MRT, larger area under curve (AUC), and significantly lower clearance rate (CL) than free CHA. These results demonstrate that Man-PEG-Lipo can act as a CHA reservoir in blood conferring a prolonged circulation time, which is advantageous for the tumor accumulation via enhanced permeability and retention (EPR) effect.

Since CHA is rapidly metabolized and cleared in vivo, CHA injections were administered intramuscularly daily for 28 days in clinical trials. Considering the pharmacokinetic characteristics of CHA, the antitumor effects of CHA were first evaluated in a G422 glioma murine model using successive administration (Fig. 6A). As shown in Fig. 6B, the chemotherapeutic agent TMZ dramatically reduced the tumor weight after oral administration compared to the control group, indicating that the G422 glioma murine model was established successfully. Moreover, free CHA was able to inhibit tumor growth after intravenous administration of 20 mg/kg daily for 14 days. As expected, the three kinds of CHA-encapsulated liposomes tested in this study also showed significant antitumor activities against G422 tumors after successive administration, with TGI% values on day 14 of 42.0%, 53.0%, and 60.3%, respectively (Fig. 6C and D). The superior antitumor efficacy of CHA-encapsulated Man-PEG-Lipo, which had the highest TGI% among the three groups, may be attributed to the TAMs-targeting effect of Man-PEG-Lipo.

To evaluate the safety of CHA and CHA-loaded liposomes, bodyweight monitoring and hematological examination were performed after successive administration for 14 days. The bodyweight of CHA-treated mice increased at the end of the experiment compared with that before treatment (Fig. 6E). In addition, free CHA and CHA-loaded liposomes did not cause significant changes in hematological indexes, including the level of white blood cells (WBC), red blood cells (RBC), and platelet (PLT) (Fig. S4), indicating that there was almost no cytotoxic effect to mice after successive administration of CHA and CHA-loaded liposomes.

3.8. In vivo antitumor efficacy of interval administration

Although the above finding and the phase I clinical trial report confirm that CHA has obvious antitumor effects on glioma following successive administration, poor patient compliance induced by successive administration represents a troublesome problem that cannot be ignored. To investigate whether Man-PEG-Lipo inhibits tumor growth following interval administration, the established G422 glioma murine model was treated with CHA-encapsulated liposomes once every other day for about two weeks according to the schedule of administration illustrated in Fig. 7A. The frequency of interval administration was half

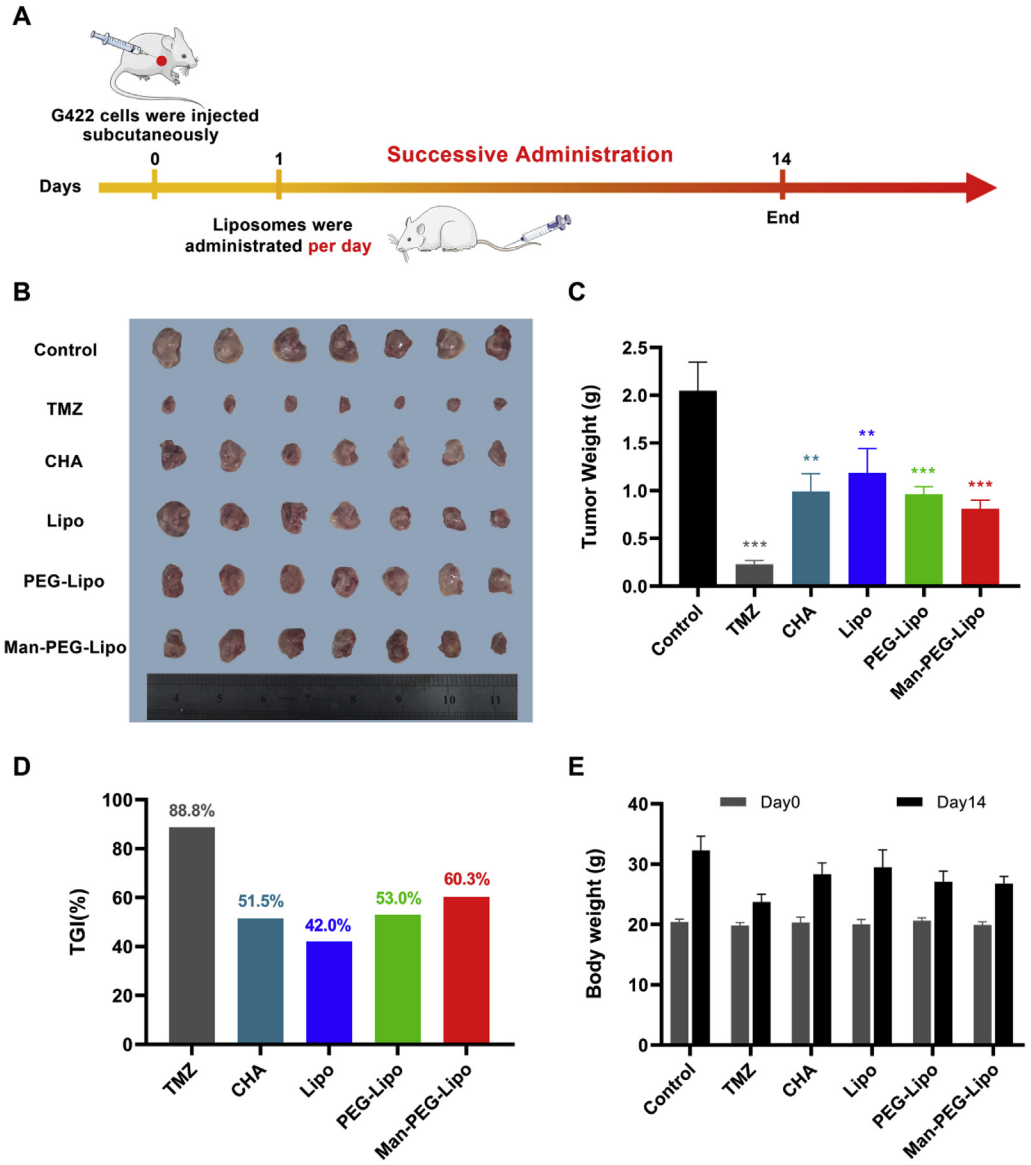

Fig. 6. In vivo antitumor efficacy and safety evaluation of CHA-encapsulated liposomes using successive administration. (A) The schematic of treatment schedule. The images of excised tumors (B), tumor weight (C), tumor growth inhibition ratio (TGI%) (D), and body weight changes (E) of murine G422 glioma tumor-bearing mice after successive intravenous treatment of CHA-encapsulated liposomes. Each value represents the mean ± SEM (n = 7). **p < 0.01 and ***p < 0.001 compared with the control group.

of that of the successive administration procedure mentioned above.

As shown in Fig. 7B, C and D, the tumor volume and tumor weight of the chemotherapeutic agent TMZ group were significantly decreased compared to those of the control group. Unlike successive administration, the tumor volume and tumor weight of mice treated with interval administration of free CHA were comparable with that of mice in the control group, demonstrating that free CHA did not inhibit glioma growth when following an interval administration regimen. The differences in the antitumor effect of free CHA between successive and interval administration may be attributed to the rapid metabolic elimination characteristic and the low tumor accumulation of free CHA in vivo. Similar to free CHA, CHA-encapsulated Lipo did not exhibit antitumor effects on the G422 glioma murine model when an interval administration procedure was followed. Compared to free CHA and CHA-encapsulated Lipo, CHA-encapsulated PEG-Lipo suppressed tumor growth to some extent, which may be ascribed to the improved tumor accumulation of PEG-Lipo via EPR effects (Fig. 5). Interestingly, compared to the modest tumor inhibition of PEG-Lipo, CHA-encapsulated Man-PEG-Lipo exhibited superior antitumor efficacy, as evidenced by the decreased tumor volume and tumor weight. These tumor volume and tumor weight values were comparable to those of TMZ, the first-line drug for glioma in the clinic (Fig. 7C and D). The remarkable antitumor efficacy of Man-PEG-Lipo may be due to enhanced tumor accumulation, selective delivery of CHA to macrophages, and sustained intracellular release.

Toxicity was evaluated by direct observations of animal behavior and body weight. Mice treated with TMZ reduced body weight and exhibited sparse hair initially after treatment, which were likely symptoms of the cytotoxic effects of chemotherapeutics. Interestingly, all mice treated with free CHA and CHA-encapsulated liposomes tolerated the regimens well. As shown in Fig. 7E, there were obvious increases in body weight in the CHA-treated mice, indicating that the immunotherapy of 20 mg/kg CHA exhibited almost no systemic toxicity.

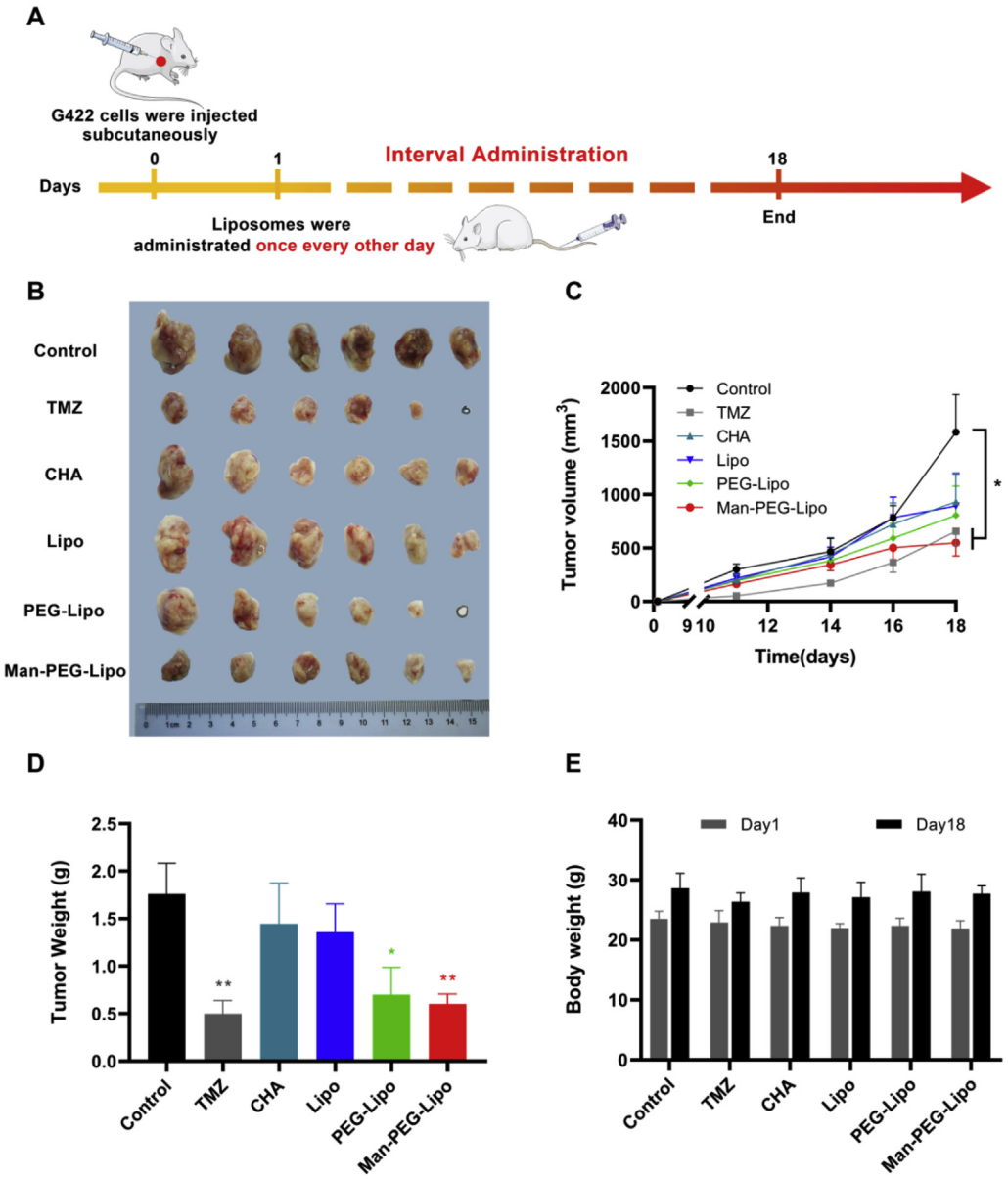

Fig. 7. In vivo antitumor efficacy and safety evaluation of CHA-encapsulated liposomes using interval administration. (A) The schematic of treatment schedule. The images of excised tumors (B), tumor volume changes (C), tumor weight (D), and body weight changes (E) of murine G422 glioma tumor-bearing mice after interval intravenous treatment of CHA-encapsulated liposomes. Each value represents the mean ± SEM (n = 6). *p < 0.05, **p < 0.01, and ***p < 0.001 compared with the control group.

3.9. Polarization ability of liposomes in vivo

The above-mentioned results of the in vitro cytotoxicity study demonstrated that free CHA and CHA-encapsulated liposomes exhibited no cytotoxicity to the mouse macrophage cell line RAW264.7 (Fig. 4A). Additionally, a previous study reported that CHA induced almost no cytotoxic effects toward tumor cells at concentrations lower than 10 μM [6]. Therefore, we investigated whether the encouraging therapeutic effects of Man-PEG-Lipo stemmed principally from the immunoregulatory ability of CHA to promote the polarization of M2-type to M1-type macrophages. The in vivo polarization ability of CHA-encapsulated liposomes was evaluated by analyzing the ratio of M1/M2 subtype macrophages, cytokine production, and the expression profile of surface proteins and gene marker.

Flow cytometry assays were carried out to quantitatively determine the number of TAMs of the different phenotypes in both tumor and spleen tissues: M2-type and M1-type TAMs were distinguished by possessing $F4/80^+CD206^+$ and $F4/80^+CD11c^+$, respectively. As expected, flow cytometer analysis demonstrated that only Man-PEG-Lipo could elevate the amount of M1 macrophages and reduce the amount of M2 macrophages in both tumor and spleen tissues, whereas the other groups had no effect on the number of the different macrophages phenotypes (Fig. 8). To better evaluate the in vivo polarization ability of Man-PEG-Lipo, the ratios of M1/M2 were calculated. An increased ratio of M1/M2 is associated with an improved polarization effect [19]. As shown in Fig. 8D and G, the ratio of M1/M2 in both tumor and spleen tissues of the Man-PEG-Lipo-treated group was significantly higher than that of other treatment groups, indicating that Man-PEG-Lipo effectively promoted the polarization of M2-type to M1-type TAMs.

Previous studies reported that most of TAMs arose from the spleen resident macrophages and circulating monocytes derived from bone marrow [51–53]. Particularly, macrophages derived from the spleen at the stage of tumor development were found to polarize toward M2-type

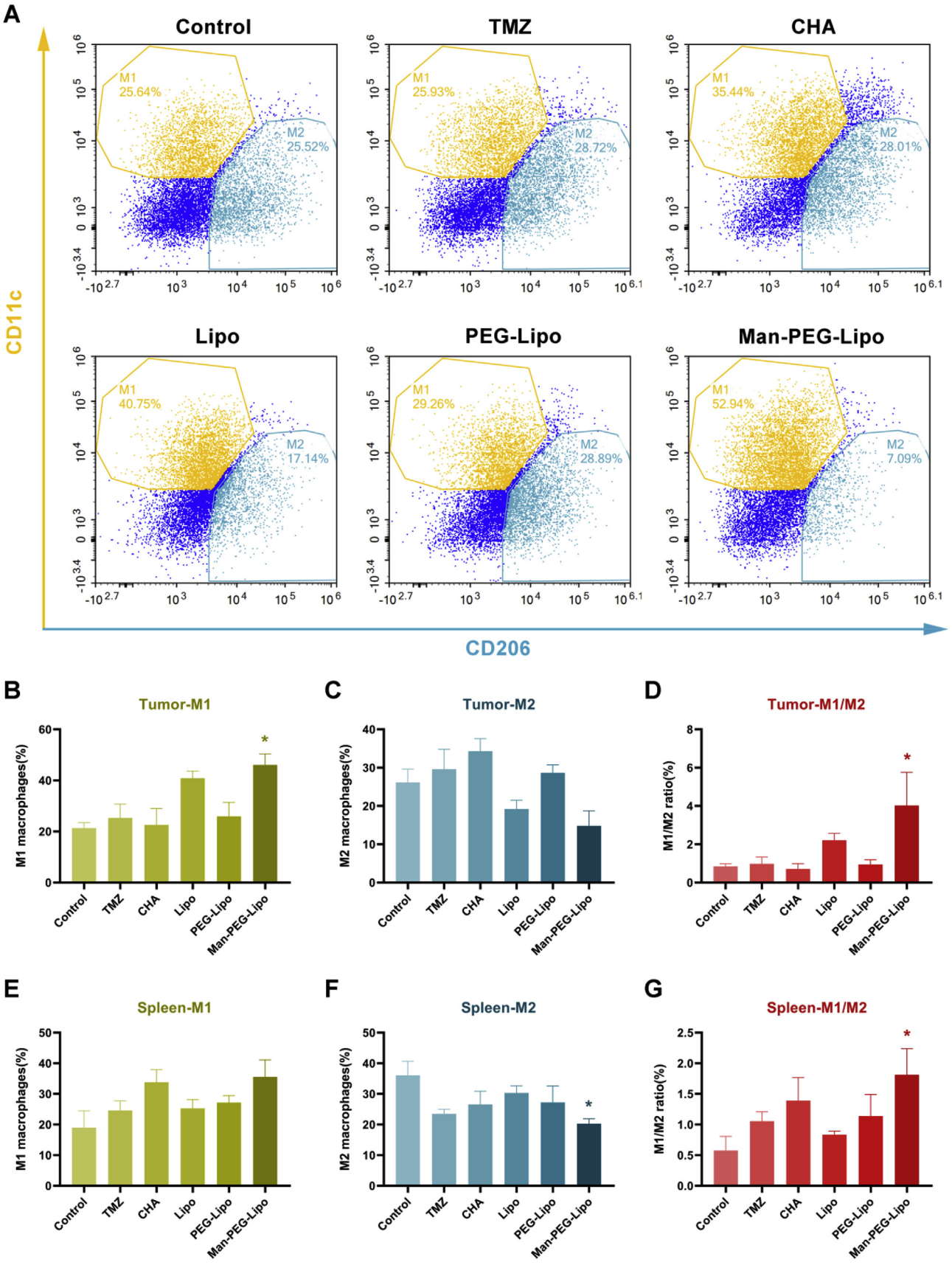

Fig. 8. The in vivo polarization ability of CHA-encapsulated liposomes was evaluated by analyzing the ratio of M1/M2 subtype macrophages in both tumor and spleen tissues. (A) Flow cytometric analysis of the TAMs phenotype in tumor tissues. The amount of M1-type TAMs (B), M2-type TAMs (C), and the ratio of M1/M2 subtype TAMs (D) in tumor tissues. The amount of M1-type TAMs (E), M2-type TAMs (F), and the ratio of M1/M2 subtype macrophages (G) in spleen tissues. Each value represents the mean ± SEM (n = 3). *p < 0.05 compared with the control group.

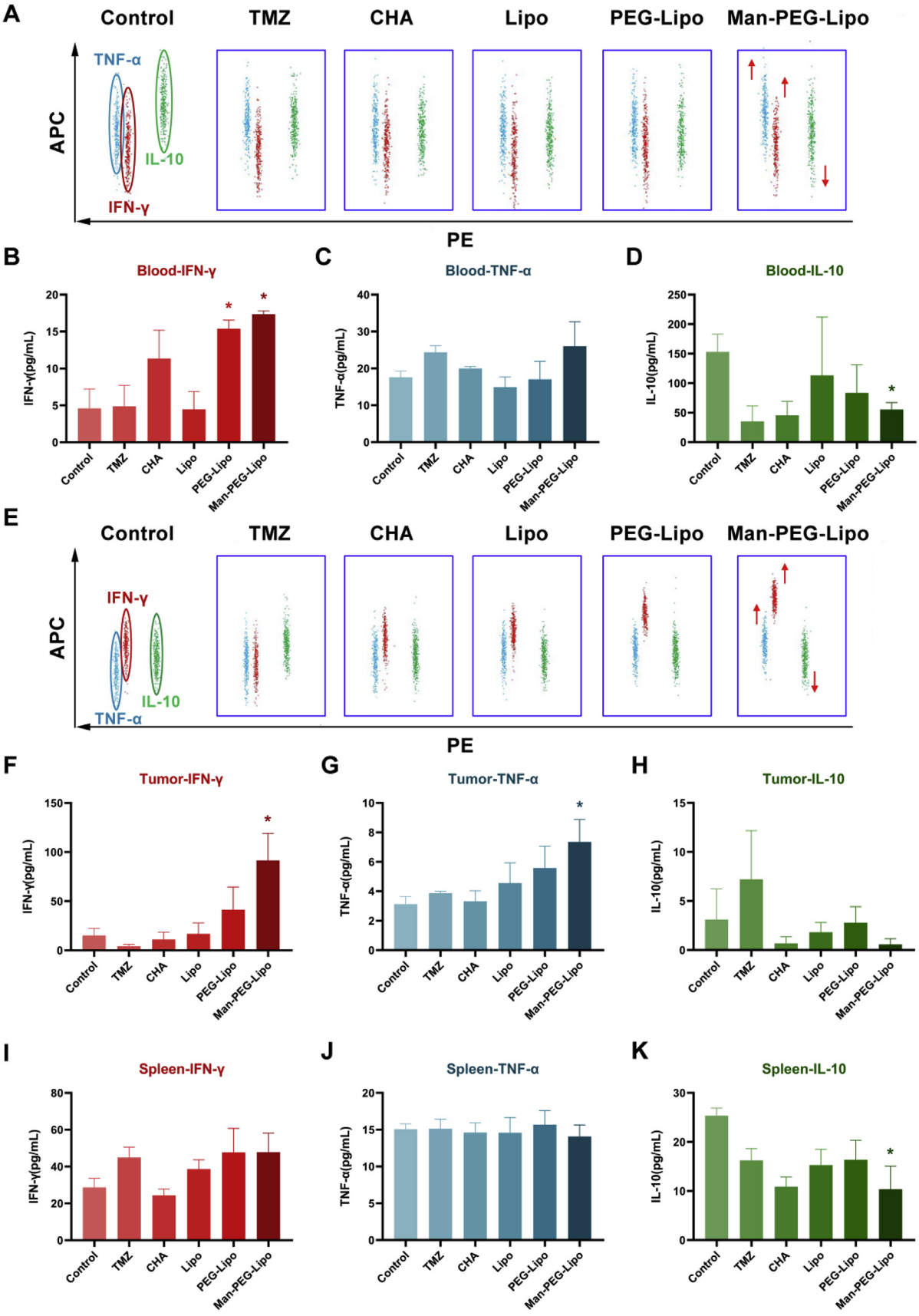

Fig. 9. The in vivo polarization ability of CHA-encapsulated liposomes was evaluated by analyzing the cytokine production. (A) Flow cytometric dot plots of cytokine production induced by CHA-encapsulated liposomes in blood. Cytokine secretion of IFN-γ (B), TNF-α (C), and IL-10 (D) in blood. (E) Flow cytometric dot plots of cytokine production induced by CHA-encapsulated liposomes in tumor tissues. Cytokine secretion of IFN-γ (F), TNF-α (G), and IL-10 (H) in tumor tissues. Cytokine secretion of IFN-γ (I), TNF-α (J), and IL-10 (K) in spleen tissues. Each value represents the mean ± SEM (n = 3). *p < 0.05 compared with the control group.

macrophages [54]. In addition, a great number of TAMs could physically relocate from the spleen to the tumor stroma and then promote tumor progression [53]. As spleen resident macrophages have been identified to contribute to the pool of TAMs in tumor, promoting the polarization of M2-type to M1-type macrophages in spleen is also of great significance for improving the antitumor immune response of Man-PEG-Lipo as compared to that in tumor sites.

M1-type macrophages facilitate an immunological response against tumors by producing immunogenic cytokines, such as IFN-γ and TNF-α. On the contrary, M2-type macrophages promote tumor growth by enhancing the release of immunosuppressive cytokine IL-10 [4,55]. Thus, the secreted cytokines were identified to further confirm the effect of Man-PEG-Lipo on the polarization of TAMs. It was noted that treatment with Man-PEG-Lipo elevated the production of IFN-γ and TNF-α and decreased the secretion of IL-10 in both peripheral blood and tumor tissues (Fig. 9). Although Man-PEG-Lipo had no impact on TNF-α production in spleen tissues, the levels of IFN-γ and IL-10 in the spleen had the same variation trend in the peripheral blood and tumor tissues (Fig. 9I, J, and K).

Apart from the analysis of the ratio of M1/M2 subtype macrophages, the expression profiles of surface proteins (CD86 for M1-type, CD206 for M2-type) and gene marker (iNOS mRNA for M1-type) on TAMs was determined by immunofluorescence and quantitative real-time PCR to verify the polarization ability of Man-PEG-Lipo. As shown in Fig. S5A, the expression level of the M2 phenotype TAMs surface marker CD206 was significantly reduced in the Man-PEG-Lipo-treated group compared to the control group. Besides, Man-PEG-Lipo induced pronounced upregulation of CD86 expression along with iNOS mRNA expression compared to the control group (Figs. S5A and B). The expression profiles of surface proteins were consistent with the results of the ratio of M1/M2 subtype macrophages, further confirming the polarization ability of Man-PEG-Lipo.

4. Conclusion

In the study, we developed CHA-encapsulated liposomes modified with mannose, which could selectively deliver CHA to TAMs for cancer immunotherapy of GBM. The prepared CHA-encapsulated mannosylated liposomes were highly effective at targeting TAMs and in promoting the polarization of the pro-tumorigenic M2 phenotype to the anti-tumorigenic M1 phenotype, thereby inhibiting G422 glioma tumor growth. Therefore, CHA-encapsulated mannosylated liposomes present a potential strategy for TAMs-targeted cancer immunotherapy of GBM with negligible systemic toxicity.

CRediT authorship contribution statement

Jun Ye: Conceptualization, Methodology, Investigation, Formal analysis, Writing - original draft. **Yanfang Yang:** Conceptualization, Investigation, Writing - review & editing. **Jing Jin:** Resources, Validation. **Ming Ji:** Resources, Validation. **Yue Gao:** Investigation, Validation. **Yu Feng:** Investigation, Validation. **Hongliang Wang:** Writing - review & editing. **Xiaoguang Chen:** Supervision, Project administration, Writing - review & editing. **Yuling Liu:** Supervision, Project administration, Funding acquisition, Writing - review & editing.

Declaration of competing interest

The authors have declared that no competing interest exists.

Acknowledgments

This work was financially supported by the National Science and Technology Major Project of China (Grant No. 2018ZX09721003 and 2018ZX09711001), the Fundamental Research Funds for the Central Universities (Grant No. 3332019069) and the Young Scientists Fund of the National Natural Science Foundation of China (Grant No. 81703566).

Appendix A. Supplementary data

Supplementary data to this article can be found online at https://doi.org/10.1016/j.bioactmat.2020.05.001.

References

[1] P.Y. Wen, D.A. Reardon, Neuro-oncology in 2015: progress in glioma diagnosis, classification and treatment, Nat. Rev. Neurol. 12 (2) (2016) 69–70.
[2] A. Rape, B. Ananthanarayanan, S. Kumar, Engineering strategies to mimic the glioblastoma microenvironment, Adv. Drug Deliv. Rev. 79 (2014) 172–183.
[3] D.G. DeNardo, B. Ruffell, Macrophages as regulators of tumour immunity and immunotherapy, Nat. Rev. Immunol. 19 (6) (2019) 369–382.
[4] Y. Singh, V.K. Pawar, J.G. Meher, K. Raval, A. Kumar, R. Shrivastava, S. Bhadauria, M.K. Chourasia, Targeting tumor associated macrophages (TAMs) via nanocarriers, J. Contr. Release 254 (2017) 92–106.
[5] D. Hambardzumyan, D.H. Gutmann, H. Kettenmann, The role of microglia and macrophages in glioma maintenance and progression, Nat. Neurosci. 19 (1) (2016) 20–27.
[6] N. Xue, Q. Zhou, M. Ji, J. Jin, F. Lai, J. Chen, M. Zhang, J. Jia, H. Yang, J. Zhang, W. Li, J. Jiang, X. Chen, Chlorogenic acid inhibits glioblastoma growth through repolarizating macrophage from M2 to M1 phenotype, Sci. Rep. 7 (2017) 39011.
[7] M. Ovais, M. Guo, C. Chen, Tailoring nanomaterials for targeting tumor-associated macrophages, Adv. Mater. 31 (19) (2019) e1808303.
[8] N.T. Trac, E.J. Chung, Peptide-based targeting of immunosuppressive cells in cancer, Bioact, Materials 5 (1) (2020) 92–101.
[9] J. Gan, Y. Dou, Y. Li, Z. Wang, L. Wang, S. Liu, Q. Li, H. Yu, C. Liu, C. Han, Z. Huang, J. Zhang, C. Wang, L. Dong, Producing anti-inflammatory macrophages by nanoparticle-triggered clustering of mannose receptors, Biomaterials 178 (2018) 95–108.
[10] Y. Zhang, L. Wu, Z. Li, W. Zhang, F. Luo, Y. Chu, G. Chen, Glycocalyx-mimicking nanoparticles improve anti-PD-L1 cancer immunotherapy through reversion of tumor-associated macrophages, Biomacromolecules 19 (6) (2018) 2098–2108.
[11] P. Chaubey, B. Mishra, Mannose-conjugated chitosan nanoparticles loaded with rifampicin for the treatment of visceral leishmaniasis, Carbohydr. Polym. 101 (2014) 1101–1108.
[12] M. Muthiah, H. Vu-Quang, Y.-K. Kim, J.H. Rhee, S.H. Kang, S.Y. Jun, Y.-J. Choi, Y.Y. Jeong, C.-S. Cho, I.-K. Park, Mannose-poly(ethylene glycol)-linked SPION targeted to antigen presenting cells for magnetic resonance imaging on lymph node, Carbohydr. Polym. 92 (2) (2013) 1586–1595.
[13] J. Ye, Y. Yang, W. Dong, Y. Gao, Y. Meng, H. Wang, L. Li, J. Jin, M. Ji, X. Xia, X. Chen, Y. Jin, Y. Liu, Drug-free mannosylated liposomes inhibit tumor growth by promoting the polarization of tumor-associated macrophages, Int. J. Nanomed. 14 (2019) 3203–3220.
[14] M.K. Sabnani, R. Rajan, B. Rowland, V. Mavinkurve, L.M. Wood, A.A. Gabizon, N.M. La-Beck, Liposome promotion of tumor growth is associated with angiogenesis and inhibition of antitumor immune responses, Nanomed. Nanotechnol. Biol. Med. 11 (2) (2015) 259–262.
[15] R. Rajan, M.K. Sabnani, V. Mavinkurve, H. Shmeeda, H. Mansouri, S. Bonkoungou, A.D. Le, L.M. Wood, A.A. Gabizon, N.M. La-Beck, Liposome-induced immunosuppression and tumor growth is mediated by macrophages and mitigated by liposome-encapsulated alendronate, J. Contr. Release 271 (2018) 139–148.
[16] D. Reichel, M. Tripathi, J.M. Perez, Biological effects of nanoparticles on macrophage polarization in the tumor microenvironment, Nanotheranostics 3 (1) (2019) 66–88.
[17] X. Zang, X. Zhang, X. Zhao, H. Hu, M. Qiao, Y. Deng, D. Chen, Targeted delivery of miRNA 155 to tumor associated macrophages for tumor immunotherapy, Mol. Pharm. 16 (4) (2019) 1714–1722.
[18] X. Zang, X. Zhang, H. Hu, M. Qiao, X. Zhao, Y. Deng, D. Chen, Targeted delivery of zoledronate to tumor-associated macrophages for cancer immunotherapy, Mol. Pharm. 16 (5) (2019) 2249–2258.
[19] T. Wang, J. Zhang, T. Hou, X. Yin, N. Zhang, Selective targeting of tumor cells and tumor associated macrophages separately by twin-like core-shell nanoparticles for enhanced tumor-localized chemoimmunotherapy, Nanoscale 11 (29) (2019) 13934–13946.
[20] L. Pang, Y. Pei, G. Uzunalli, H. Hyun, L.T. Lyle, Y. Yeo, Surface modification of polymeric nanoparticles with M2pep peptide for drug delivery to tumor-associated macrophages, Pharm. Res. (N. Y.) 36 (4) (2019) 65.
[21] M. Naveed, V. Hejazi, M. Abbas, A.A. Kamboh, G.J. Khan, M. Shumzaid, F. Ahmad, D. Babazadeh, X. FangFang, F. Modarresi-Ghazani, L. WenHua, Z. XiaoHui, Chlorogenic acid (CGA): a pharmacological review and call for further research, Biomed. Pharmacother. 97 (2018) 67–74.
[22] L.-L.W. Shuai Huang, Ni-Na Xue, Cong Li, Hui-Hui Guo, Tian-Kun Ren, Yun Zhan, Wen-Bing Li, Jie Zhang, Xiao-Guang Chen, Yan-Xing Han, Jin-Lan Zhang, Jian-Dong Jiang, Chlorogenic acid effectively treats cancers through induction of cancer cell differentiation, Theranostics 9 (23) (2019) 6780–6796.
[23] W. Li, M. Ji, N. Xue, Z. Kang, X. Kang, S. Li, X. Chen, First in human phase I study of chlorogenic acid injection in recurrent high grade glioma, J. Clin. Oncol. 36

(15_suppl) (2018) e14081-e14081.
[24] Q. Li, L.X. Sun, L. Xu, Y. Jia, Z.W. Wang, Z.D. Shen, K.S. Bi, Determination and pharmacokinetic study of syringin and chlorogenic acid in rat plasma after administration of Aidi lyophilizer, Biomed. Chromatogr. 20 (12) (2006) 1315–1320.
[25] J. Zhang, M. Chen, W. Ju, S. Liu, M. Xu, J. Chu, T. Wu, Liquid chromatograph/tandem mass spectrometry assay for the simultaneous determination of chlorogenic acid and cinnamic acid in plasma and its application to a pharmacokinetic study, J. Pharmaceut. Biomed. Anal. 51 (3) (2010) 685–690.
[26] Y. Li, X. Ren, C. Lio, W. Sun, K. Lai, Y. Liu, Z. Zhang, J. Liang, H. Zhou, L. Liu, H. Huang, J. Ren, P. Luo, A chlorogenic acid-phospholipid complex ameliorates post-myocardial infarction inflammatory response mediated by mitochondrial reactive oxygen species in SAMP8 mice, Pharmacol. Res. 130 (2018) 110–122.
[27] I. Pineda-Torra, M. Gage, A. de Juan, O.M. Pello, Isolation, culture, and polarization of murine bone marrow-derived and peritoneal macrophages, Methods Mol. Biol. 1339 (2015) 101–109.
[28] X. Qi, Y.n. Dong, H. Wang, C. Wang, F. Li, Application of Turbiscan in the homo-aggregation and heteroaggregation of copper nanoparticles, Colloid. Surface. Physicochem. Eng. Aspect. 535 (2017) 96–104.
[29] Y. Ono, M. Nagai, O. Yoshino, K. Koga, A. Nawaz, H. Hatta, H. Nishizono, G. Izumi, A. Nakashima, J. Imura, K. Tobe, T. Fujii, Y. Osuga, S. Saito, CD11c+ M1-like macrophages (MΦs) but not CD206+ M2-like MΦ are involved in folliculogenesis in mice ovary, Sci. Rep. 8 (1) (2018) 8171.
[30] S. Morgan, Q. Wang, C. Harberg, B. Liu, Macrophage phenotypes in murine aneurysm, Faseb. J. 27 (1_supplement) (2013) lb487-lb487.
[31] C. Ngambenjawong, H.H. Gustafson, S.H. Pun, Progress in tumor-associated macrophage (TAM)-targeted therapeutics, Adv. Drug Deliv. Rev. 114 (2017) 206–221.
[32] Y. Barenholz, S. Amselem, D. Goren, R. Cohen, D. Gelvan, A. Samuni, E.B. Golden, A. Gabizon, Stability of liposomal doxorubicin formulations: problems and prospects, Med. Res. Rev. 13 (4) (1993) 449–491.
[33] B. Heurtault, P. Saulnier, B. Pech, J.-E. Proust, J.-P. Benoit, Physico-chemical stability of colloidal lipid particles, Biomaterials 24 (23) (2003) 4283–4300.
[34] Y. Sun, A. Deac, G.G.Z. Zhang, Assessing physical stability of colloidal dispersions using a turbiscan optical analyzer, Mol. Pharm. 16 (2) (2019) 877–885.
[35] C. Marianecci, D. Paolino, C. Celia, M. Fresta, M. Carafa, F. Alhaique, Non-ionic surfactant vesicles in pulmonary glucocorticoid delivery: characterization and interaction with human lung fibroblasts, J. Contr. Release 147 (1) (2010) 127–135.
[36] B. Liu, Y. Zhu, J. Tian, T. Guan, D. Li, C. Bao, W. Norde, P. Wen, Y. Li, Inhibition of oil digestion in Pickering emulsions stabilized by oxidized cellulose nanofibrils for low-calorie food design, RSC Adv. 9 (26) (2019) 14966–14973.
[37] D.D. Lasic, F.J. Martin, A. Gabizon, S.K. Huang, D. Papahadjopoulos, Sterically stabilized liposomes: a hypothesis on the molecular origin of the extended circulation times, Biochim. Biophys. Acta Biomembr. 1070 (1) (1991) 187–192.
[38] D. Papahadjopoulos, T.M. Allen, A. Gabizon, E. Mayhew, K. Matthay, S.K. Huang, K.D. Lee, M.C. Woodle, D.D. Lasic, C. Redemann, Sterically stabilized liposomes: improvements in pharmacokinetics and antitumor therapeutic efficacy, Proc. Natl. Acad. Sci. Unit. States Am. 88 (24) (1991) 11460–11464.
[39] F. Danhier, O. Feron, V. Preat, To exploit the tumor microenvironment: passive and active tumor targeting of nanocarriers for anti-cancer drug delivery, J. Contr. Release 148 (2) (2010) 135–146.
[40] Y. Yan, N. Liu, N. Hou, L. Dong, J. Li, Chlorogenic acid inhibits hepatocellular carcinoma in vitro and in vivo, J. Nutr. Biochem. 46 (2017) 68–73.
[41] F. Zhang, G. Yin, X. Han, X. Jiang, Z. Bao, Chlorogenic acid inhibits osteosarcoma carcinogenesis via suppressing the STAT3/Snail pathway, J. Cell. Biochem. 120 (6) (2019) 10342–10350.
[42] K. Yamagata, Y. Izawa, D. Onodera, M. Tagami, Chlorogenic acid regulates apoptosis and stem cell marker-related gene expression in A549 human lung cancer cells, Mol. Cell. Biochem. 441 (1) (2018) 9–19.
[43] N. Hou, N. Liu, J. Han, Y. Yan, J. Li, Chlorogenic acid induces reactive oxygen species generation and inhibits the viability of human colon cancer cells, Anti Canc. Drugs 28 (1) (2017) 59–65.
[44] Y. Wang, Y.-X. Lin, S.-L. Qiao, J. Wang, H. Wang, Progress in tumor-associated macrophages: from bench to bedside, Adv. Biosys. 3 (2) (2019) 1800232.
[45] I.F. Parney, J.S. Waldron, A.T. Parsa, Flow cytometry and in vitro analysis of human glioma–associated macrophages, J. Neurosurg. 110 (3) (2009) 572–582.
[46] A.C. Carvalho da Fonseca, B. Badie, Microglia and macrophages in malignant gliomas: recent discoveries and implications for promising therapies, Clin. Dev. Immunol. 2013 (2013) 264124.
[47] H.J. Byeon, L.Q. Thao, S. Lee, S.Y. Min, E.S. Lee, B.S. Shin, H.-G. Choi, Y.S. Youn, Doxorubicin-loaded nanoparticles consisted of cationic- and mannose-modified-albumins for dual-targeting in brain tumors, J. Contr. Release 225 (2016) 301–313.
[48] X. Ying, H. Wen, W.-L. Lu, J. Du, J. Guo, W. Tian, Y. Men, Y. Zhang, R.-J. Li, T.-Y. Yang, D.-W. Shang, J.-N. Lou, L.-R. Zhang, Q. Zhang, Dual-targeting daunorubicin liposomes improve the therapeutic efficacy of brain glioma in animals, J. Contr. Release 141 (2) (2010) 183–192.
[49] X.-Y. Li, Y. Zhao, M.-G. Sun, J.-F. Shi, R.-J. Ju, C.-X. Zhang, X.-T. Li, W.-Y. Zhao, L.-M. Mu, F. Zeng, J.-N. Lou, W.-L. Lu, Multifunctional liposomes loaded with paclitaxel and artemether for treatment of invasive brain glioma, Biomaterials 35 (21) (2014) 5591–5604.
[50] P. Zhao, W. Yin, A. Wu, Y. Tang, J. Wang, Z. Pan, T. Lin, M. Zhang, B. Chen, Y. Duan, Y. Huang, Dual-targeting to cancer cells and M2 macrophages via biomimetic delivery of mannosylated albumin nanoparticles for drug-resistant cancer therapy, Adv. Funct. Mater. 27 (44) (2017) 1700403.
[51] R.A. Franklin, W. Liao, A. Sarkar, M.V. Kim, M.R. Bivona, K. Liu, E.G. Pamer, M.O. Li, The cellular and molecular origin of tumor-associated macrophages, Science 344 (6186) (2014) 921–925.
[52] P. Tymoszuk, H. Evens, V. Marzola, K. Wachowicz, M.H. Wasmer, S. Datta, E. Muller-Holzner, H. Fiegl, G. Bock, N. van Rooijen, I. Theurl, W. Doppler, In situ proliferation contributes to accumulation of tumor-associated macrophages in spontaneous mammary tumors, Eur. J. Immunol. 44 (8) (2014) 2247–2262.
[53] V. Cortez-Retamozo, M. Etzrodt, A. Newton, P.J. Rauch, A. Chudnovskiy, C. Berger, R.J.H. Ryan, Y. Iwamoto, B. Marinelli, R. Gorbatov, R. Forghani, T.I. Novobrantseva, V. Koteliansky, J.-L. Figueiredo, J.W. Chen, D.G. Anderson, M. Nahrendorf, F.K. Swirski, R. Weissleder, M.J. Pittet, Origins of tumor-associated macrophages and neutrophils, Proc. Natl. Acad. Sci. Unit. States Am. 109 (7) (2012) 2491–2496.
[54] O.M. Karaman, A.V. Ivanchenko, V.F. Chekhun, Macrophages - a perspective target for antineoplastic immunotherapy, Exp. Oncol. 41 (4) (2019) 282–290.
[55] P. Jeannin, L. Paolini, C. Adam, Y. Delneste, The roles of CSFs on the functional polarization of tumor-associated macrophages, FEBS J. 285 (4) (2018) 680–699.
[56] X. Wu, Y. Zhang, X. Chen, G. Liu, G. Chen, M. Jiang, Glycocalyx-Mimicking Nanoparticles for Stimulation and Polarization of Macrophages via Specific Interactions, Small 11 (33) (2015) 4191–4200, https://doi.org/10.1002/smll.201403838.